The bacteria-protist link as a main route of dissolved organic matter across contrasting productivity areas on the Patagonian Shelf

M. Celeste López-Abbate[1], John E. Garzón-Cardona[1,2], Ricardo Silva[3], Juan-Carlos Molinero[4], Laura A. Ruiz-Etcheverry[5,6,7], Ana M. Martínez[8], Azul S. Gilabert[1,9], Rubén J. Lara[1]

[1] Instituto Argentino de Oceanografía (CONICET-UNS), Camino La Carrindanga km 7.5, 8000 Bahía Blanca, Argentina.

[2] Departamento de Química, Universidad Nacional del Sur, 8000 Bahía Blanca, Argentina.

[3] Instituto Nacional de Investigación y Desarrollo Pesquero (INIDEP), B7602HSA, Mar del Plata, Buenos Aires, Argentina.

[4] Institut de Recherche pour le Développement (IRD), UMR248 MARBEC, IRD/CNRS/IFREMER/UM, Sète Cedex, France.

[5] Departamento de Ciencias de La Atmósfera y Los Océanos, Facultad de Ciencias Exactas y Naturales, Universidad de Buenos Aires (DCAO, FCEN-UBA), Ciudad Universitaria, Pabellón II 2do. Piso, C1428EGA Ciudad Autónoma de Buenos Aires, Argentina

[6] Centro de Investigaciones Del Mar y La Atmósfera (CIMA/CONICET-UBA), C1428EGA Ciudad Autónoma de Buenos Aires, Argentina

[7] Instituto Franco-Argentino para El Estudio Del Clima y Sus Impactos (IRL-IFAECI/CNRS-CONICET-UBA), C1428EGA Ciudad Autónoma de Buenos Aires, Argentina

[8] Instituto de Química del Sur (INQUISUR-CONICET), Universidad Nacional del Sur, 8000 Bahía Blanca, Argentina.

[9] Departamento de Geografía y Turismo (DGyT), Universidad Nacional del Sur, 8000 Bahía Blanca, Argentina.

Correspondence to: Celeste López-Abbate (mclabbate@iado-conicet.gob.ar)

Abstract

While the sources of dissolved organic matter (DOM) in the open ocean are relatively well identified, its fate due to microbial activity is still evolving. Here, we explored how microbial community structure, growth, and grazing of phytoplankton and heterotrophic bacteria influenced the DOM pool and the transformation of its fluorescent fraction. Dilution experiments were performed during the productive season on the Patagonian Shelf (SW Atlantic Ocean), a region of intense biological activity, with peak productivity observed at the shelf break front. Although phytoplankton biomass was higher than that of bacteria, protists selectively preyed on the faster-growing bacterial population, denoting trophic specificity of grazers. High trophic coupling was suggested by the biomass distribution of protistan consumers and their prey, which predominantly exhibited an inverted trophic pyramid structure. An exception to this pattern was observed at the highly productive shelf break front, where a traditional bottom-heavy pyramid emerged, indicating that most phytoplankton evaded protist predation despite evidence of herbivory. Bacterial consumption of DOM appeared uncoupled from its total amount but was influenced by DOM complexity, while the bacterial production of humic-like substances from protistan plankton precursors observed in most experiments highlighted a potential pathway for carbon sequestration. Protistan grazers also significantly influenced DOM dynamics by scaling their DOM contribution in response to the intensity of grazing on heterotrophic bacteria, regardless of productivity levels. This effect likely arises from reducing the number of active, DOM-consuming bacteria and by providing egestion DOM compounds. At the onset of the productive season, high bacterial growth rates stimulate protistan grazing, which serve as a link between bacterial biomass and higher trophic levels. However, as grazing pressure increases, protists can also contribute to the accumulation of a fraction of DOM.

1.   Introduction

Dissolved organic matter (DOM), the second-largest carbon reservoir in the ocean after dissolved inorganic carbon, is subject to dynamic regulation by physical and biological processes (Spencer et al., 2007). Unveiling the nature and dynamics of DOM is essential for gaining deeper understanding of the biochemical pathways through which carbon circulates in marine ecosystems. The optical properties of DOM serve as a marker for its sources and biological reactivity, with chromophoric DOM reflecting phytoplankton production and fluorescence DOM (FDOM) revealing potential sources and biological and photochemical interactions (Stedmon et al., 2003; Romera-Castillo et al., 2010).

Phytoplankton are primary contributors to DOM, yet processes such as viral lysis and protistan grazing also play substantial roles in shaping its composition and quantity. Protistan grazers not only recycle nutrients and enhance bloom sustainability but also impact carbon cycling through DOM production via biomass reworking and excretion (Kujawinski et al., 2004; Baña et al., 2014; Moran et al. 2022). In addition, grazers influence DOM pools by exhibiting selective feeding behaviors regarding bacterial and phytoplanktonic prey. For example, while size-specific grazing prompt compositional shifts in phytoplankton (e.g., Kanayama et al., 2020), the more generalist grazing on bacteria implies that community structure remains relatively unchanged under grazing pressure (Baltar et al., 2016). On the other hand, grazing on bacteria seems to remain close to bacterial production, specially under oligotrophic conditions (Sanders et al., 1992), while phytoplankton may temporally scape protistan grazing under favourable growth conditions thus allowing for bloom formation (Irigoien et al., 2005). This results in varying trophic transfer efficiency between phytoplankton- and bacteria-based food webs, with the former typically involving fewer carbon steps before reaching microcrustaceans (Berglund et al., 2007).

The Patagonian Shelf, one of the world's largest continental shelf regions, serves as a hotspot for carbon cycling due to its high productivity and dynamic mixing processes that connect the euphotic zone with bottom sediments (Laruelle et al., 2018). One of its defining features is a 2,500 km-long upwelling front at the shelf break, known for recurrent spring blooms and significant biogeochemical transformations that contribute to global carbon sequestration (Romero et al., 2006; Kahl et al., 2017). The emergence of an acidification trend in the water masses adjacent to the shelf is likely linked to ongoing carbon dioxide (CO_2) capture, especially in the northern area of the shelf (Orselli et al., 2018).

Our study aimed to evaluate the role of protists in transferring bacterial and phytoplankton biomass under different productivity conditions and to assess potential changes in the chromophoric fraction of DOM–primarily representing aromatic organic compounds–and FDOM in these scenarios. We found that protistan grazing selectively targeted bacteria under both productivity regimes, and that intense grazing pressure on bacteria may contribute to the short-term accumulation of DOM substances, irrespective of productivity levels. These findings enhance our understanding of the ecological mechanisms influencing carbon flow in marine ecosystems.

2. Material and Methods

2.1 Sample collection and analyses

Two groups of stations were selected in the mid-shelf (stations 23, 22 and 21 from the coast to the open ocean) and the shelf break front (stations 14, 13 and 12 from the coast to the open ocean). Mid-shelf stations were separated by ca. 30 km intercepting the 50 m isobath, while shelf break front stations were separated by ca. 18 km and intercepted the 100 and 200 m isobaths. According to the bioregionalization of the Patagonian shelf waters proposed by Delgado et al. (2023), mid-shelf stations were located in low to moderate productivity regions (mean chlorophyll-a concentration during the spring peak between 1.14 and 2.48 µg L^{-1}), while the shelf break front stations were nested in the upwelling, highly productive region (mean chlorophyll-a concentration during the spring peak of 5.8 µg L^{-1}). Hydrographic data (temperature, salinity, pressure, and fluorescence) were taken with a SBE9plus CTD profiler during the cruise H0917 from October 9 to 12, 2017. Water samples for dissolved nutrients and for running the experiments were taken from the chlorophyll-a maximum with 6 L Niskin bottles attached to the CTD rosette, while dissolved organic carbon (DOC) samples were taken in the surface layer (5 m). The measurement of inorganic nutrients (NO_2^-, NO_3^- and NH_4^+, PO_4^{3-}, and SiO_4^{2-}), was carried out by analyzing 50 mL aliquots of seawater preserved with $HgCl_2$ solution (Kattner and Becker, 1991). The concentration of dissolved inorganic nitrogen (DIN) was calculated as the sum of NO_2^-, NO_3^- and NH_4^+. Filtered (Whatman GF/F glass fiber filters with 0.7 µm pore size.) samples for DOC were collected in pre-combusted 20 mL glass vials and acidified to pH < 2 with H_3PO_4. Filtrates were analyzed using high-temperature (680°C) catalytic oxidation with Al_2O_3 particles containing 0.5% platinum (Pt) in a TOC analyzer (Dohrmann DC-190, CA, USA). The resulting CO_2 was then quantified using non-dispersive linearized infrared gas analysis (Skoog et al., 1997).

2.2 Satellite chlorophyll-a

The spring phytoplankton bloom is a recurrent feature of the Patagonian Shelf and shelf break (e.g., Delgado et al., 2023). A time series of satellite-derived chlorophyll-a was constructed to capture the bloom timing at each station during the sampling period. We here define blooming conditions as periods where the net rate of biomass change (specific division rate minus specific loss rate) remains positive long enough to result in net biomass accumulation (Behrenfeld and Boss 2018). Factors like wind stress that may influence plankton aggregation are not considered contributors to these conditions. Moderate Resolution Imaging Spectroradiometer (MODIS) Aqua images of chlorophyll-a concentration were downloaded from the National Aeronautics and Space Administration (NASA) ocean color web site (https://oceancolor.gsfc.nasa.gov/). Daily Level 3 images with a spatial resolution of 4 km were obtained for the period spanning August 2017 to December 2017, capturing the closest pixel to each sampling point. To minimize the percentage of missing values, we computed the 5-day mean and applied a low-pass filter to remove the variability lower than 28 days.

2.3 Experimental setup

Feeding experiments, based on the dilution technique (Landry and Hassett, 1982), were prepared by gently mixing different percentages of unfiltered water and filtered water through <0.2 µm Whatman polycarbonate

124   filters. Four dilution treatments (D) were prepared using the filtered and unfiltered water: 10%, 40%, 70% and

125   100% (whole water). Water was pre-filtered by a 200 µm mesh net to eliminate larger metazoan grazers. Acid-

126   cleaned, 1 L glass experimental bottles (3 replicates) were daily (24 h) deployed at a deck-incubator (200 L)

127   equipped with continuous in situ water flow and covered with a double knitted mesh fabric (~215 g of fabric

128   per m^2) to attenuate the UV radiation. Dissolved inorganic nutrients were added to the incubation bottles

129   following the recommendations by Calbet and Saiz (2018) to ensure phytoplankton growth at non-limiting

130   conditions. Assuming moderate phytoplankton growth rates and maximum chlorophyll-a concentrations of 2

131   µg L^{-1} in the mid-shelf region and 6 µg L^{-1} in the shelf break front (Delgado et al., 2023), we supplemented the

132   water with 8.3 µM of nitrogen and silicon, and 0.5 µM of phosphorus in the mid-shelf area, and 24.9 µM of

133   nitrogen and silicon, and 1.5 µM of phosphorus in the shelf break front. A series of triplicate dilution bottles

134   without added nutrients was set as control treatment.

135   Subsamples from the initial and final treatments were collected for chlorophyll-a and bacteria abundance

136   analyses. To determine chlorophyll-a, samples (300 mL) were filtered through Whatman GF/F glass fiber filters

137   with 0.7 µm pore size. and stored at -20°C. Pigments were extracted with 90% acetone for 24 h in the dark at -

138   20° C and then determined spectrophotometrically according to Jeffrey and Humphrey (1975). Heterotrophic

139   bacteria were quantified by staining 1 mL seawater sample with 4,6-diamidino-2-phenylindole (DAPI) to a final

140   concentration of 3 µg mL^{-1} and collected on black polycarbonate filters (25 mm diameter, 0.2 µm pore size).

141   The enumeration was done with a Nikon Eclipse 80i microscope equipped with a fluorescence lamp at 100X

142   magnification and using a UV excitation filter (330-385 nm). Twenty-five images were taken at random points

143   from each polycarbonate filter using a Nikon DXM1200F digital camera and subsequently, every cell in the

144   image was enumerated and sized using the software ImageJ. Bacterial cell volumes were calculated assigning

145   simple geometric shapes to species (coccos, bacillus), and converted into carbon content (µg C L^{-1}) by the

146   allometric model according to Simon and Azam (1989).

147   Plankton samples were collected from the initial treatments to characterize the community structure at the

148   starting conditions. For the analysis of plankton in the 2–5 µm size range, triplicate samples (3 mL) were fixed

149   with 0.53 mL of glutaraldehyde (f.c. 2 %) and subsequently processed following the methods described by

150   Porter and Feig (1980). The same procedure was applied for plankton in the 5–20 µm size range, using duplicate

151   100 mL samples for counting. The identification of organisms was done by a combination of light and epi-

152   fluorescent microscopy. Preserved samples were stained with DAPI (f.c. 5 µg mL^{-1}) and proflavine (f.c. 5 µg

153   mL^{-1}) and collected on black polycarbonate filters (25 mm diameter, 0.2 µm pore size). Most taxa were

154   identified using a blue excitation filter (450-490 nm) while Cryptophytes were identified using a green

155   excitation filter (480-550 nm). Cell enumeration was done by settling the preserved sample (1-2 mL) in

156   Utermöhl chambers during 24 h. The entire chamber was analyzed under a Wild M20 inverted light microscope.

157   Similarly, the enumeration of plankton in the size fraction 20-200 µm was done by settling a variable volume

158   (50–100 mL, depending on sediment and plankton concentration) of preserved water sample (Lugol's iodine)

159   in Utermöhl chambers during 24 h. It is worth mentioning that since samples were pre-filtered through a 200

160   µm mesh to exclude larger consumers from our experiments, colony-forming protists may have been removed.

161   Biomass estimation involved assigning simple geometric shapes to species to quantify cell volume, which was

162 subsequently converted into carbon content (µg C L^{-1}) according to Hillebrand et al. (1999). Protistan taxa
163 abundance was visualized by a heatmap (employing the R package *heatmaply*). Heterotrophic and autotrophic
164 taxa were segmented into groups based on size, distinguishing between nanoplankton (2-20 µm) and
165 microplankton (20-200 µm) (Sieburth et al., 1978). Nanoplankton included heterotrophic nanoplankton (HNP),
166 coccolithophores, and phototrophic nanoplankton (PNP), while the microplankton comprised ciliates,
167 heterotrophic dinoflagellates (HD), phototrophic dinoflagellates (PD), and diatoms. Additionally, HNP
168 comprised both flagellates and ciliates, while PNP encompassed dinoflagellates, diatoms, and flagellates. A
169 side dendrogram was included to group similar sampling stations by ordering rows (stations) so that the sum of
170 distances between each one will be minimized. Data for ranking rows was normalized to range from 0 to 1. To
171 identify the dominant taxa contributing to station ordination, a biplot based on non-metric Multi-Dimensional
172 Scaling (MDS) was created using the R package *vegan.*
173 An additional treatment of pre-filtered (Whatman GF/F glass fiber filters with 0.7 µm pore size.) and undiluted
174 water was set to separate protists and measure the absorbance at 254 nm and FDOM. This was aimed to compare
175 the DOM pool at the initial and final incubation conditions in the presence (i.e., in unfiltered, undiluted
176 treatment) and in the absence of protists (i.e., in pre-filtered by 0.7 µm, undiluted treatment). Biotic effects are
177 known to produce DOM transformations in short timescales. For instance, significant shifts in both the
178 chromophoric and fluorescent fractions of DOM driven by biological processes were identifiable after 24 h
179 (Urban-Rich et al., 2004; Lønborg et al., 2010; 2015), while DOM transformation driven by bacteria occurred
180 within the first 24 h upon their release by phytoplankton (Gruber et al., 2006; Hach et al., 2020). The optical
181 properties of FDOM were evaluated from emission-excitation matrices (EEM) obtained with a Shimadzu RF-
182 5301 scanning spectrofluorometer with a 150 W xenon lamp and a 1 cm quartz cell. Milli-Q water was used as
183 reference and the intensity of the Raman peak was regularly checked. The emission wavelength ranged between
184 250 nm and 600 nm while the excitation wavelength ranged between 220 nm and 370 nm. Dissolved humic-
185 like and protein-like substances were estimated using the wavelengths proposed by Coble (1996). Humic-like
186 material was represented by three fluorophores: $FDOM_C$ (Ex/Em: 350/440) and $FDOM_A$ (Ex/Em: 250/425) of
187 terrestrial origin, and $FDOM_M$ (Ex/Em: 310/380) of marine origin. $FDOM_C$ indicates highly unsaturated
188 components, $FDOM_A$ reflects a moderate degree of unsaturation, and $FDOM_M$ suggests a low degree of
189 unsaturation. Protein-like material was characterized by two fluorophores: $FDOM_B$ (Ex/Em: 260/300) and
190 $FDOM_T$ (Ex/Em: 270/330), both derived from autochthonous biogenic sources. $FDOM_B$ is associated with
191 compounds similar to tryptophan and tyrosine, linked to recent organic matter production through primary
192 productivity, while $FDOM_T$ indicates tryptophan-like compounds formed from microbial protein breakdown
193 (Jørgensen et al., 2011; Drozdova et al., 2022). Fluorescence intensity of fluorophores was expressed in
194 Arbitrary Units (AU). Fluorophores were identified using the PARAFAC multivariate algorithm (Stedmon and
195 Bro, 2008), and different biogeochemical indicators such as humification index (HIX), fluorescence index (FI),
196 and freshness index (BIX), were calculated (Coble, 1996). The HIX serves as a tool for assessing the degree of
197 humification in DOM, which reflects its aromaticity and the extent of diagenetic alteration (Bai et al., 2015),
198 while the FI distinguishes between DOM of different origins, i.e., terrestrial vs. microbial (McKnight et al.,

2001). The BIX aims to estimate the relative contribution of DOM produced in situ by microbes (Huguet et al., 2009).

The absorbance spectra between 240 to 800 nm were measured in a Perkin Elmer Lambda 35 spectrophotometer. The absorbance at 254 nm (a254) from the chromophoric fraction of DOM was used as a proxy of the DOM amount (Brandstetter et al., 1996). Absorbance at 254 nm represents 50–60% of the carbon content in marine DOM (Görs et al., 2007). It primarily includes unsaturated compounds with aromatic rings, conjugated systems, or carbonyl groups, mostly of biological relevance such as aromatic amino acids, nucleic acids, photosynthetic pigments, and steroids (Martínez-Pérez et al., 2017). As a result, a254–although not representing all DOC present–can be used as reliable proxy for the evolution of DOM concentration during incubation experiments. Net changes in the a254 fraction of DOM across the incubation time were calculated as $1/t \ln (a254)t/(a254)0$, where $(a254)0$ and $(a254)t$ are the a254 nm at the initial (0) and final (t) conditions, respectively. Lee et al. (2018) identified parameters with more than a 50% absolute percent difference between the control and treated samples as reliable indicators to distinguish between DOM transformation caused by biodegradation, UV irradiance, and adsorption. Here we used the tendency during incubation of BIX, HIX, FI, and the ratio between FDOM components M and A ($FDOM_M/FDOM_A$) as reliable parameters for the discrimination of biodegradation versus UV photodegradation or adsorption. Pairwise relationship between net changes in a254 in the presence and absence of protists with variables of interest, was evaluated by simple regression models. The same procedure was used with other variables to test for pairwise relationships of ecological significance.

2.4 Phytoplankton and bacterial growth and grazing by phagotrophic protists

Rate estimates of phytoplankton growth (μ) and mortality due to protist grazing (m) were obtained using the equations of Landry and Hassett (1982). While initially intended for measuring phytoplankton growth and mortality, we adapted this method to assess bacterial growth rate and bacterivory. This approach has been demonstrated to be effective and reliable for use with natural bacterial communities in non-oligotrophic regions (Tremaine and Mills, 1987). The method is based on measuring the initial and final concentration of chlorophyll-a (as a proxy of phytoplankton biomass) and bacterial abundance in triplicate dilution series after an incubation period of 24 h. It assumes that protistan grazing rate is a linear function of prey concentration (Holling type I functional response), and can be calculated as follows:

$$\mu_0 = 1/t \ln Pt/P0 = \mu - mD$$

where μ_0 is the apparent growth rate, P0 and Pt are the phytoplankton concentration at the initial (0) and final (t) conditions, respectively, D is the dilution series. The m:μ ratio x 100 was used to calculate the percentage of the daily bacterial/primary productivity consumed by protistan grazers. We tested model fit by linear regression analysis in every experiment.

3.   Results

3.1   Phytoplankton phenological stages at the sampling area

Mean surface chlorophyll-a, derived from satellite observations during the sampling period (October 9-12, 2017, Fig. 1a), revealed a band of high phytoplankton concentration at the shelf break front, centred at the 114 m isobath in the latitudinal band at 40°S. While the spring bloom typically begins during September in the latitudinal range of our sampling area (Delgado et al., 2023), phytoplankton at the time of sampling, as estimated from satellite chlorophyll-a, were at different phenological stages in each station (Fig. 1b). At the mid-shelf, station 21 showed the highest concentration of satellite chlorophyll-a and the phytoplankton community was at the pulse initiation. Stations 22 and 23 showed lower chlorophyll-a and were sampled at bloom stationary phase. At the shelf break front, satellite-derived chlorophyll-a levels were elevated in stations 13 and 14, indicating proximity to the bloom peak, whereas station 12 exhibited low chlorophyll-a concentration, corresponding to the bloom termination phase.
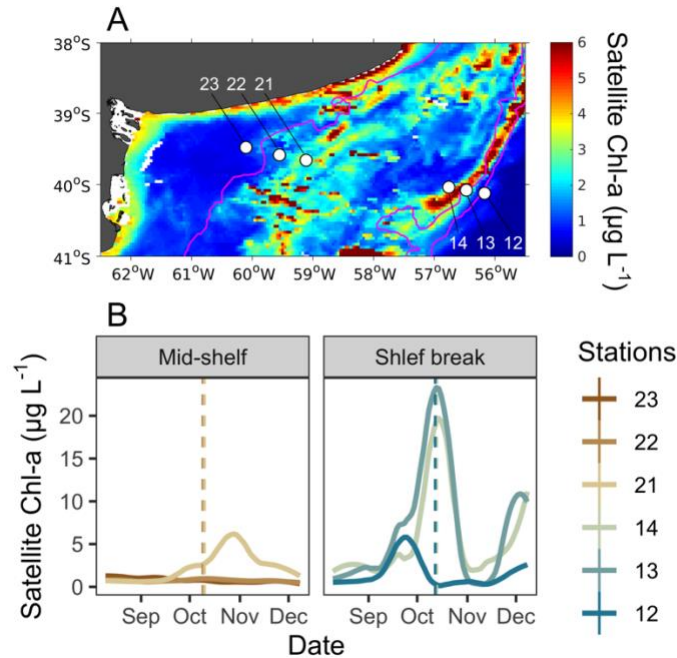
Figure 1.A. Map of the study site showing the location of sampling stations (white dots) and the mean surface distribution of satellite chlorophyll-a (Chl-a) during the sampling period (October 09-12). Stations 23, 22 and 21 were located in the mid-shelf area, and stations 14, 13 and 12 were located in the shelf break front. B. Temporal evolution of surface satellite Chl-a concentration at grid points closest to sampling stations in the mid-shelf and the shelf break front. Solid lines denote satellite Chl-a concentration at each station, while dashed lines represent the date of in situ sampling. Lines are color-coded according to the symbols representing each station.

3.2 Hydrography, nutrients, and DOM properties

Thermohaline signature was in the range of the Subantarctic Shelf waters ($33.5 < S < 34$) from station 21 to station 14 in agreement with Berden et al. (2020) and Ferronato et al. (2023). At the mid-shelf area, station 23 and 22 showed relatively higher salinity values ($S > 33.7$), linked to the coastal maximum salinity waters originating at San Matias Gulf (Lucas et al., 2005). These stations also showed weak stratification, while the rest of the stations showed a sharper thermocline. The mixed layer depth (MLD) was shallower (10 m) in stations 12 and 23, whereas in all other stations, it averaged 30 m. All samples taken at the chlorophyll-a maximum were positioned within the mixed layer.

The concentration of dissolved nutrients (DIN, PO_4^{3-} and SiO_4^{2-}) was highest at station 12, while the lowest total nutrient concentration was recorded at station 23 (Fig. 2). The primary nitrogen source was NO_3^-, except for station 22 where NH_4^+ predominated. The only notable distinction between station groups was the concentration of NO_3^-, which averaged 1.2 µM in the mid-shelf stations and 7.3 µM in the shelf break front stations. According to Redfield ratios (Redfield et al., 1963), a strong nitrogen depletion in relation to PO_4^{3-} and SiO_4^{2-} occurred in station 23. While the N:P ratio was closer to 16:1 in the rest of the stations, a general excess of PO_4^{3-} in relation to DIN was registered. On the contrary, all stations except for station 23, showed a Si depletion in relation to DIN. The concentration of DOC in surface waters was homogeneous in the mid-shelf stations (mean of 79 µM), while in the shelf break it varied from 96 µM, in station 14, to 52 µM, in station 13 (Fig. 2). The highest fluorescence intensity of protein-like compounds ($FDOM_T$ and $FDOM_B$) was found in station 23, while the highest intensity of humic-like fluorophores was observed in station 21 (Fig. 3). The a254 was higher in the mid-shelf stations (mean of 2.3 m^{-1}) compared to the shelf break front stations (mean of 1.3 m^{-1}).
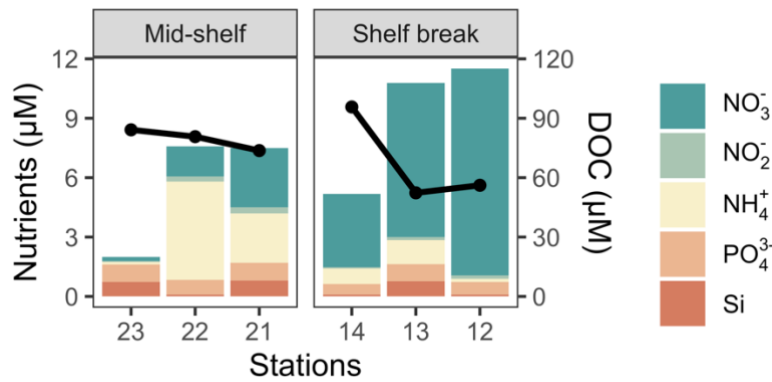
Figure 2. Cumulative nutrient concentrations at the deep chlorophyll-a maximum (bars) and the concentration of DOC in surface waters (solid black line) across stations in the mid-shelf and the shelf break front.

285
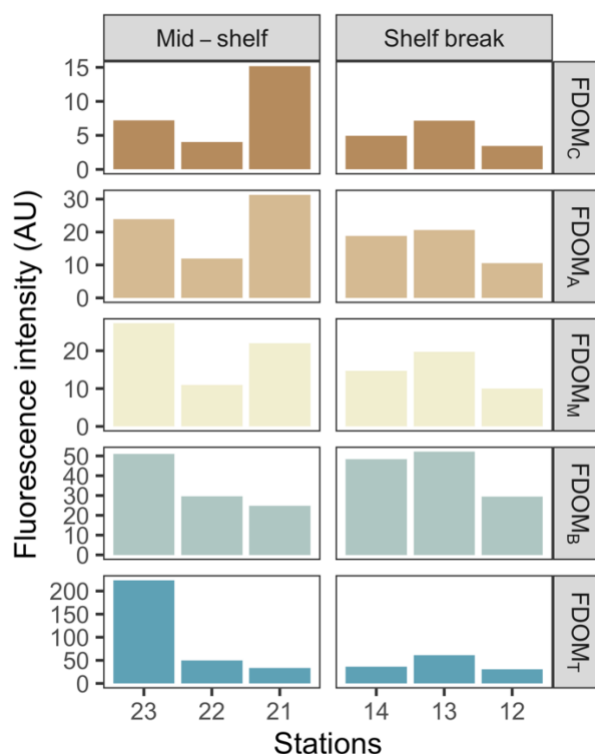
Figure 3. Fluorescence intensity of main identified FDOM components at the deep chlorophyll-a maximum across stations in the mid-shelf and the shelf break front. FDOM components are shown in a decreasing order of humification from top to bottom plots.

289

3.3 Plankton community structure

290

The biomass of protistan grazers exceeded that of phytoplankton and heterotrophic bacteria at most sampling stations, except at stations 13 and 14, where phytoplankton biomass dominated (Fig. 4a). Heterotrophic dinoflagellates dominated the biomass across stations, except at station 14, where HNP prevailed. In contrast, no clear distribution pattern was observed among phytoplankton groups. Biomass of heterotrophic bacteria ranged between 2.6 (station 22) and 15 µg C L^{-1} (station 14) (Fig. 4b). The abundance of this group was positively associated with chlorophyll-a concentration (R^2=0.7, p=0.04) and the abundance and biomass of most phytoplankton groups (p<0.05), except coccolithophores. The highest bacterial abundance and biomass was registered under chlorophyll-a pulse initiation (stations 21, 13 and 14). Among protistan grazers, the most significant group in terms of biomass were dinoflagellates ranging from 0 (station 14) to 134 µg C L^{-1} (station 22, mostly due to the presence of *Noctiluca scintillans*). Ciliates ranged from 0 (station 14) to 20 µg C L^{-1} (station 21), while HNP showed the highest biomass in stations 13 and 14 (5 and 6 µg C L^{-1}, respectively), and the lowest value was registered in station 12 (0.6 µg C L^{-1}). Plankton <5 µm (choanoflagellates and other unidentified flagellates) was the dominant fraction among HNP except in station 13, were micro-sized ciliates and nano-sized flagellates (*Telonema* sp. and unidentified dinoflagellates) dominated biomass.

305

306
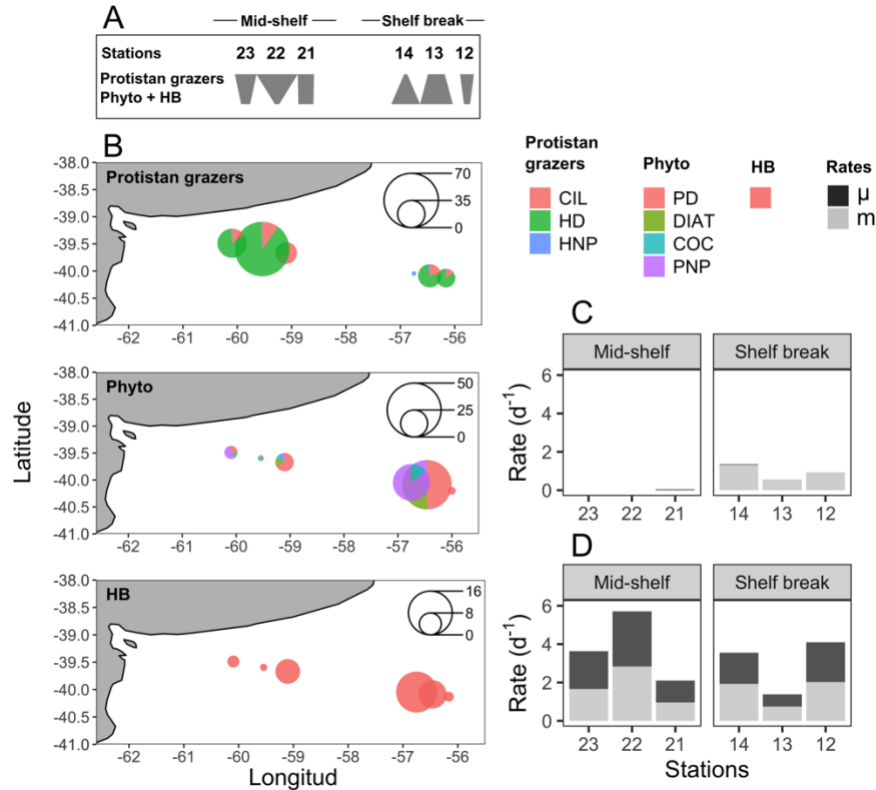
307 **Figure 4.A. Polygons represent the type of food web structure based on the ranking of carbon biomass**

308 **of protistan grazers, phytoplankton (phyto), and heterotrophic bacteria (HB) in each sampling station**

309 **(indicated above the polygons), adapted from Kang et el. (2023). Inverted or top-heavy pyramids (stations**

310 **23, 22, 21 and 12), occur when the biomass of protistan grazers surpasses that of their prey**

311 **(phytoplankton plus HB). In contrast, the more conventional bottom-heavy structure (stations 14 and**

312 **13), are characterized by a greater prey biomass relative to that of consumers. B. Spatial distribution of**

313 **the cumulative biomass (μg C L^{-1}) of protistan grazers (upper plot), phytoplankton (mid-plot) and HB**

314 **(lower plot). Scale circles are shown within each plot. C. Growth (μ) and grazing (m) rates of**

315 **phytoplankton. D. Growth (μ) and grazing (m) rates of HB.**

316

317 The biomass of photosynthetic taxa was generally dominated by PNP. The highest concentration and biomass

318 of all groups, except for coccolithophores, was registered in station 13 (PNF: 32 μg C L^{-1}, PD: 8 μg C L^{-1},

319 diatoms: 6 μg C L^{-1}). High biomass of PNP and dinoflagellates was also registered in station 14 (34 μg C L^{-1})

320 and station 21 (8.5 μg C L^{-1}), respectively. The highest biomass of coccolithophores was registered in station

321 22 (2 μg C L^{-1}).

322 Stations 12 and 13 showed differences on microplankton community structure compared to the rest of the

323 stations (Fig. 5). According to the ordination fit between vectors (i.e., taxa) and stations, the protistan grazers

324 that mainly contributed to separate these two stations from the others were the dinoflagellates *Gymnodinum*

325 spp., and *Protoperidinium pellucidum*, while *Pyramimonas* sp. and *Dinophysis acuminata*, were the distinctive

326 photosynthetic species in these stations (MDS, p<0.05). Stations 22 and 23 were also closely associated

327 regarding the protistan grazers community and the species that contributed most to this association was

328 *Strombidinopsis* sp.

329

330
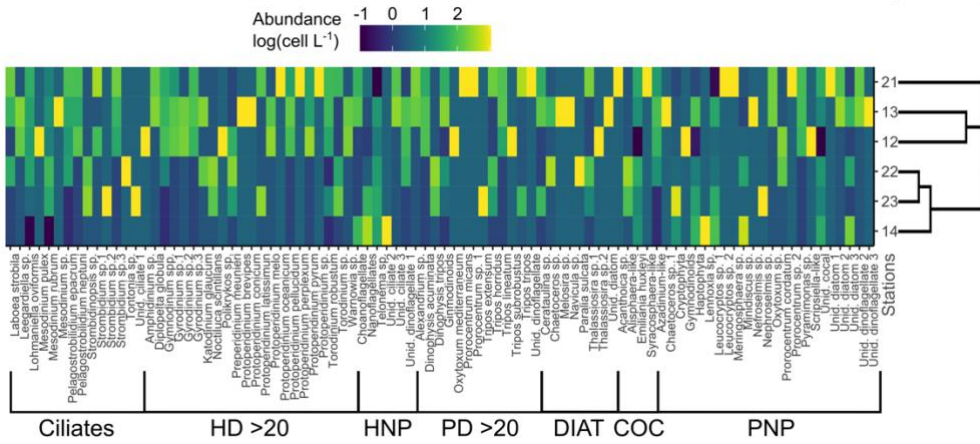
331 **Figure 5. Color-coded, log-transformed cell abundance (cell L^{-1} × 10^3) of plankton taxa (columns) at the**

332 **sampling stations (rows). Group delimitation is indicated at the bottom. Side dendrogram shows the**

333 **optimal ordering of rows (stations) so that the sum of distances between each one is minimized. HD>20:**

334 **Heterotrophic dinoflagellates >20 μm, HNP: Heterotrophic nanoplankton, PD>20: Photosynthetic**

335 **dinoflagellates >20 μm, Diat: Diatoms, Coc: Coccolithophores, PNP: Photosynthetic nanoplankton.**

336

337 ### 3.4   Growth and grazing rates

338 Water temperature of the incubator container was hourly monitored and ranged between 12.2 and 13.8°C in the

339 mid-shelf stations and between 8 and 11.1°C in the shelf break stations. Bacteria showed active growth during

340 all experiments while phytoplankton only revealed significant growth rates in conditions of pulse initiation

341 (stations 21 and 14). Some degree of nutrient limitation was detected in the mid-shelf stations as the growth

342 rate of phytoplankton at the control treatments was lower than in the nutrient amended treatment, however,

343 differences were not statistically significant. No apparent differences were found in stations 12, 13 and 14.

344 Significant grazing effect on bacteria was found in all experiments (Fig. 4c), while grazing on phytoplankton

345 was only significant in the shelf break stations (Fig. 4d). In the mid-shelf stations, daily bacterial productivity

346 consumed by HNP averaged 72%, while in the shelf break stations, it reached 83%. Mean daily primary

347 productivity consumed by protistan grazers was zero in the mid-shelf stations and 155% in the shelf break.

348 Linear responses were found in all experiments, indicating that no cascading effects, saturating feeding or

349 starvation occurred within incubation bottles. The abundance of heterotrophic bacteria was negatively

350 correlated with the grazing of HNP (R^2=0.8, p=0.016) and growth (R^2=0.9, p=0.005).

351

352 ### 3.5   Short-term DOM transformations

353 An accumulation of the a254 DOM fraction was observed in stations 22, 14, 13, and 12 during the incubation

354 period in the experimental setting with protists, while stations 23 and 21 exhibited DOM consumption (Fig. 6a).

355 Conversely, in the experimental setting without protists, the a254 DOM fraction accumulated in stations 22, 21,
356 14, and 12, while stations 23 and 13 showed DOM consumption (Fig. 7a). Regardless of net DOM production,
357 biodegradation of organic matter occurred in most experiments as denoted by the decrease in the BIX and the
358 increase in the HIX (Fig. 6b, 7b). The prevalence of biodegradation over UV photodegradation or adsorption
359 was further supported by most source discrimination indices (FI and M/A, data not shown). The decrease in
360 BIX was coherent with the net zero to low phytoplankton growth during our experiments. An exception to this
361 general pattern occurred in station 13, in which HIX increased and BIX decreased during the incubation. Station
362 13 was characterized by the highest abundance of micro-sized phytoplankton (diatoms and photosynthetic
363 dinoflagellates) and registered the lowest concentration of DOC (52 µM) at the moment of sampling. While
364 HIX and BIX indices suggested that DOM modifications are not driven by biodegradation, M/A decreased and
365 FI increased during the experiments, thus giving inconsistent results.

366 Among treatments, a shift from accumulation to consumption of the a254 DOM fraction was registered in
367 stations 21 and 13. In the presence of protists, the net a254 fraction of DOM change was negatively associated
368 with the fluorescence intensity of peaks related to humic-like compounds (FDOM$_C$: R^2=0.6, p=0.07, FDOM$_A$,
369 R^2=0.8, p=0.01, FDOM$_M$: R^2=0.7, p=0.04), and positively associated with the grazing on HB (R^2=0.7, p=0.00,
370 Fig. 8a). In the absence of protists, the net a254 fraction of DOM change was negatively associated with the
371 ratio between bacteria and phytoplankton biomass (R^2=0.8, p=0.01, Fig. 8b).

372
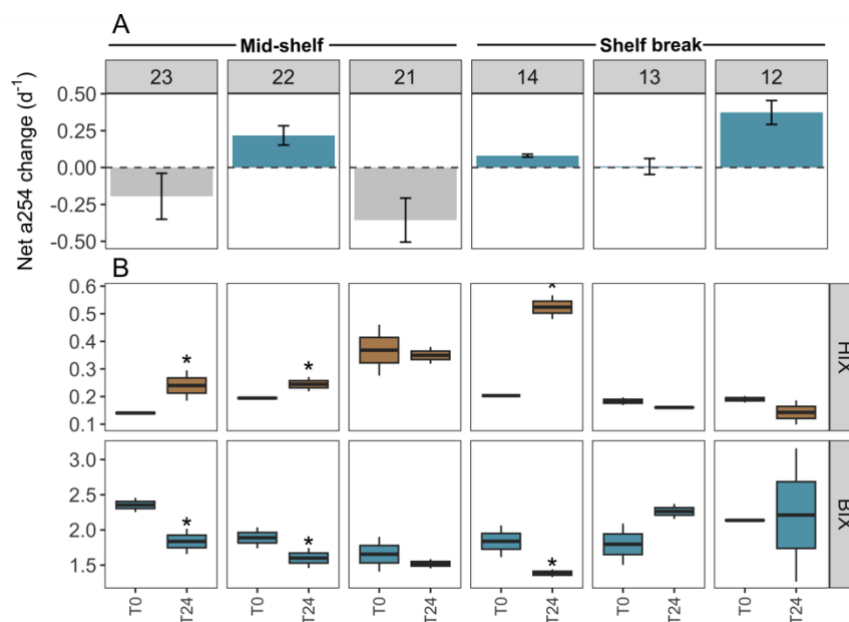
373
374 **Figure 6. DOM transformations in the experimental setting with protists (pre-filtered by 200 µm) across**
375 **stations in the mid-shelf and the shelf break front. A. Net changes in the absorbance at 254 nm (a254)**
376 **from the chromophoric fraction of DOM, a proxy of total DOM concentration. Dashed line indicates the**
377 **limit between negative (i.e., consumption) and positive net a254 changes (i.e., accumulation) during the**
378 **incubation period. B. Shifts in the humification index (HIX) and the biological activity index (BIX) during**

379 **the 24-h incubation. Asterisks indicate significant differences identified by linear regression analysis**
380 **between initial and final treatments (p<0.05).**

381

382

383 **Figure 7. DOM transformations in the experimental setting without protists (pre-filtered by 0.7 μm)**
384 **across stations in the mid-shelf and the shelf break front. A. Net changes in the absorbance at 254 nm**
385 **(a254) from the chromophoric fraction of DOM, a proxy of total DOM concentration. Dashed line**
386 **indicates the limit between negative (i.e., consumption) and positive net a254 changes (i.e., accumulation)**
387 **during the incubation period. B. Shift in the humification index (HIX) and the biological activity index**
388 **(BIX) during the 24-h incubation. Asterisks indicate significant differences identified by linear regression**
389 **analysis between initial and final treatments (p<0.05).**

390

391
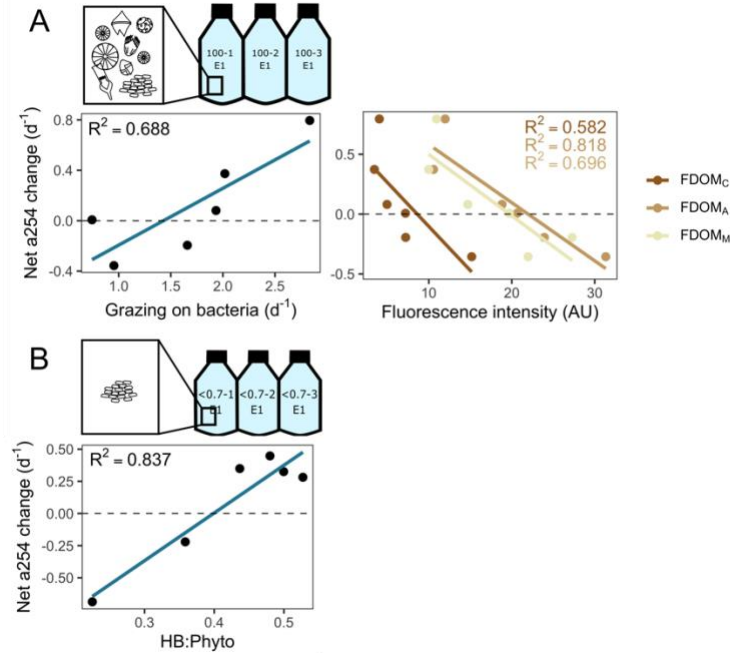
Figure 8. Main predictors of the net changes in the absorbance at 254 nm (a254) from the chromophoric fraction of DOM during incubations. A. Experimental setting with protists. Linear regression plots depict the relationship between net a254 changes and grazing on bacteria, and humic-like substances (as depicted by fluorophores FDOM$_C$, FDOM$_A$, and FDOM$_M$). B. Experimental setting without protists. Linear regression plot depicts the relationship between net a245 changes and the ratio between heterotrophic bacteria (HB) and phytoplankton (Phyto) biomass. Dashed lines indicate the limit between negative (i.e., consumption) and positive (i.e., accumulation) net a254 changes.

399

4 Discussion

4.1 Microbial food web structure

Plankton composition and distribution varied notably across blooming and non-blooming stations, with station 14 standing out for its atypical plankton structure within a bloom region. Dominated by a nanoplanktonic diatom and a small grazer community, this station also showed high bacterial biomass, likely due to low PO_4^{3-} and Si concentrations, but high DOC levels. Nanoplankton, particularly diatoms, cryptophytes, and haptophytes, were predominant across sampling stations, with cyanobacteria assumed to play a significant role in carbon fixation. Similar findings were reported in previous studies by Silva et al. (2009) and Negri et al. (2013; 2016), indicating the widespread dominance of plankton <5 µm in the region. The contrast in chlorophyll-a concentration between the upwelling and the mid-shelf areas may be related to nitrate content, which is the main limiting nutrient on the Patagonian Shelf (Paparazzo et al. 2010). The shelf break front receives a continuous supply from the nutrient-rich upwelling of the Malvinas Current, while nitrate on the mid-shelf is mainly provided from the northward flow of Subantarctic Waters. However, as it moves north, phytoplankton uptake depletes nitrate, leading to lower concentrations on the northern Patagonian Shelf (Song et al. 2016). This creates a regional contrast in nutrient levels between the shelf and the shelf break.

415 In the shelf break front, dinoflagellates dominated both photosynthetic and heterotrophic biomass, while ciliates
416 were more abundant in the mid-shelf. Besides these spatial differences, the lack of a clear distribution pattern
417 of plankton highlights the impact of mesoscale structures on spatial plankton heterogeneity (Lehahn et al.,
418 2018), a feature proper of the Patagonian Shelf (Saraceno et al., 2024). Heterotrophic bacterial abundance was
419 comparable to coastal summer values reported by Hozbor et al. (2013), Negri et al. (2016), and Garzón-Cardona
420 et al. (2021). It exhibited a positive correlation with chlorophyll-a, but was negatively affected by HNP grazing.
421 This dynamic suggests that bacterial populations are primarily regulated by grazing pressure and the availability
422 of phytoplankton-derived DOM, rather than by nutrient limitation during periods of high productivity.
423

4.2   Microbial trophic pathways

425 In oligotrophic areas, microbial food webs involve multi-step carbon transfer dominated by small organisms
426 that efficiently recycle nutrients. By contrast, productive regions have shorter, more efficient food webs where
427 carbon moves directly to higher trophic levels (Armengol et al., 2019). Our observations showed strong
428 microbial trophic coupling across the mid-shelf and the shelf break front, however under more productive
429 conditions, a fraction of primary producers escaped grazing. Mid-shelf stations, including post-bloom station
430 12, exhibited an "inverted pyramid" biomass structure, where consumer biomass exceeded that of their prey
431 suggesting high trophic efficiency, as shown in former studies (McCauley et al., 2018). In the shelf break front,
432 despite evidence of protistan herbivory, much of the phytoplankton biomass remained ungrazed likely due to
433 strong top-down pressure from microcrustaceans on both phytoplankton and protistan grazers. This created a
434 more typical bottom-heavy biomass structure, indicative of high primary productivity where some primary
435 production bypasses protist predation and is consumed by microcrustaceans or exported. Such a food web
436 configuration achieves the highest carbon biomass, regardless of community composition (Kang et al., 2023).
437 These observations align with previous findings in the shelf region, showing strong trophic coupling and
438 minimal sinking of unused biomass, dominated by small phytoplankton (<5 µm) and balanced biomass levels
439 of micro- and mesozooplankton (Negri et al., 2013).
440 Our findings showed active growth of heterotrophic bacteria across all stations, while phytoplankton exhibited
441 low net growth or biomass yield, except at two stations undergoing developing bloom stages (14 and 21).
442 Heterotrophic bacteria, despite having half the biomass of phytoplankton, was selectively preyed by protistan
443 grazers, accounting for 72% of bacterial production in mid-shelf stations and 83% in the shelf break front (Fig.
444 9). This preference for bacteria likely stems from their higher growth rate compared to phytoplankton, as
445 protistan grazing is primarily triggered by prey growth rate rather than biomass (Banse, 1982; Calbet and
446 Landry, 2004; Chen et al., 2009). Regarding the low phytoplankton growth rates observed in this study, an
447 additional factor beyond bloom timing may involve UV photoinhibition, which can affect some eukaryotic
448 pigmented plankton when exposed to deck conditions. Although light conditions were carefully controlled
449 during handling and the incubator was covered with a special net to prevent overexposure, continuous light
450 exposure cannot fully replicate the natural mitigation of UV stress provided by vertical mixing in the water
451 column (Häder et al., 2015). Laws et al. (2000) noted unrealistic growth estimates, attributing the negative
452 effects of UV exposure to phytoplankton incubation at the surface. Simulating natural UV exposure remains a

453 common challenge in most incubation experiments, where communities experience more stable light
454 conditions.

455 Our results showed that bacteria exhibited growth advantages over phytoplankton across the examined
456 environmental gradient but were concurrently more vulnerable to grazing pressure. This compensatory grazing
457 on fast-growing bacteria has been previously observed in productive environments such as the California
458 Current (Goericke, 2011; Taylor and Landry, 2018; Landry et al., 2023), as well as in the oligotrophic Warm
459 Taiwan Current (Chiang et al., 2014). The suggested mechanism underlying this trophic interaction posits that
460 increased phytoplankton-DOM production fosters the growth of resource-efficient bacteria, as suggested by the
461 tight coupling between bacteria and phytoplankton biomass. However, the heightened growth, coupled with a
462 diminished allocation of energy to defensive skills, renders these bacteria susceptible to selective grazing
463 (Landry et al. 2023).

464 The situation in the more productive shelf break front shifted toward a coupled predation upon both prokaryotes
465 and phytoplankton (Fig. 9). Grazing accounted for 83% of bacterial production and 154% of phytoplankton
466 production. Despite limited growth, phytoplankton faced substantial grazing pressure, possibly facilitated by
467 shared predators with bacteria. This trophic interaction aligns with the enhanced microbial loop hypothesis
468 (Taylor and Landry, 2018), suggesting that small phytoplankton is increasingly grazed as a byproduct of grazers
469 actively preying on bacteria under conditions of rising productivity. Under this scenario, grazing on
470 picophytoplankton is density-independent and occurs due to the presence of shared common grazers with
471 bacteria. Overall, bacteria appeared to be positively regulated by commensalism with phytoplankton and
472 negatively by grazing, constituting a primary carbon source for protistan grazers regardless of the productivity
473 level.

474 An additional factor contributing to grazing selectivity across productivity areas may be related to grazer
475 community composition, which differed between the mid-shelf and the shelf break front, with ciliates more
476 concentrated on the mid-shelf and heterotrophic dinoflagellates more associated with shelf break stations
477 (especially in stations 12 and 13). In contrast, phytoplankton structure showed no distinct regional differences.
478 Ciliates primarily select prey based on size as their oral diameter limits ingestion. They can thrive on a diet
479 composed exclusively of prey of uniform size, such as bacteria. In contrast, dinoflagellates employ diverse
480 feeding strategies, allowing them access to a broader range of prey sizes. This trait positions dinoflagellates as
481 key grazers in meso- and eutrophic environments, such as upwelling areas (e.g., Hansen et al., 1997; Sherr and
482 Sherr, 2007; Calbet, 2008), enabling them to effectively target both bacteria and larger phytoplankton.

483

4.3   Short-term DOM pathways

485 Throughout the experiments, substantial bacterial proliferation and minimal or no phytoplankton growth were
486 observed to occur alongside the active biodegradation of organic matter, as evidenced by a decrease in the
487 biological index (BIX) and an increase in the humification index (HIX). The general decreasing trend of BIX
488 during the incubation and its similar behaviour in the absence of protist confirms a bacterial effect and suggests
489 that bacteria are rapidly consuming recently produced phytoplankton exudates. Comparable observations have
490 shown that bacteria produce humic-like substances from protistan plankton precursors in controlled

491   environments absent of terrestrial influence (Gruber et al., 2006; Romera-Castillo et al., 2011; Lechtenfeld et

492   al., 2015; Kinsey et al., 2018; Osburn et al., 2019), underscoring the pivotal role of microbial communities in

493   converting DOM into refractory substances over brief timescales. The described carbon route partially explains

494   why the region acts as a carbon sink throughout most of the year (Kahl et al., 2017), irrespective of the

495   magnitude of primary productivity, and emphasize the critical role of the microbial carbon pump (Jiao et al.,

496   2010) as a key carbon sequestration pathway on the northern Patagonian Shelf. The moderate to high DOC

497   concentration compared to other open waters (Hansell et al. 2009), appears to support sustained bacteria growth.

498   While these findings highlight its importance, the seasonal relevance of this mechanism remains to be explored.

499   The accumulation of a fraction of DOM, as indicated by a254, was not limited to stations experiencing active

500   phytoplankton growth, indicating that net DOM release is not necessarily tied to specific phenological stages,

501   as previously suggested (Bachi et al., 2023). Moreover, accumulation occurred under diverse phytoplankton

502   assemblages, implying a low level of specialization in the bacterial utilization of species-specific DOM

503   substances, a trait that becomes apparent under conditions of high resource availability (Sarmento et al., 2016).

504   It is worth noting that while a254 is a reliable proxy for DOM quantity, representing 50–60% of the carbon

505   content, it primarily reflects aromatic compounds, which dominate humic substances in DOM. In contrast,

506   aliphatic compounds contribute to a lesser extent. As a result, experimental results may overlook the production

507   of simpler compounds.

508   The complexity of DOM, reflected by the prevalence of humic-like compounds (FDOM$_C$, FDOM$_A$, and

509   FDOM$_M$), emerged as a key factor influencing the bacterial utilization of DOM. A net consumption of the DOM

510   fraction, as estimated by a254, was observed when the initial DOM pool contained a significant proportion of

511   low-reactivity compounds, influenced by the phenological status of the sampling site, as indicated by satellite

512   chlorophyll-a trends. However, while stations 21 and 23 had high proportions of refractory compounds, they

513   differed in labile compound content, leading to distinct experimental outcomes. Both stations had low pre-

514   sampling chlorophyll-a, indicating limited recent autochthonous DOM production, yet showed contrasting

515   bacterial activity. In station 23, high bacterial activity increased DOM complexity and net consumption under

516   both treatments, suggesting dependence on an initial labile DOM pool (FDOM$_T$). In contrast, station 21 had

517   low bacterial activity, with the a254 DOM fraction shifting from consumption to accumulation without protists,

518   indicating bacterial reliance on phytoplankton DOM exudates when the DOM pool was predominantly

519   refractory.

520   At station 13, the opposite pattern was observed, with the a254 DOM fraction shifting from weak accumulation

521   in the presence of protists, to consumption in the absence of protists. Here, a higher proportion of labile DOM

522   facilitated bacterial activity. Low bacteria-to-phytoplankton biomass ratios indicated that bacterial DOM

523   consumption was masked by phytoplankton biomass but became evident without protists. That is, in stations

524   were bacterial biomass is low relative to phytoplankton, bacteria appear to rely more on phytoplankton-derived

525   DOM than on other sources. This effect become apparent upon removal of protists that implies the absence of

526   newly produced DOM (Fig. 8b), in which a net a254 DOM fraction consumption was observed. Overall, the

527   initial proportion of refractory compounds better predicted the net DOM production by providing insights on

528   microbial succession trajectories. While changes in DOM production and consumption in protist-free bottles

529 were mainly driven by heterotrophic bacteria, filtration likely allowed cyanobacteria and viruses to pass

530 through, contributing additional DOM. *Synechococcus*, the dominant cyanobacteria in the Patagonian Shelf,

531 releases bioavailable DOM that stimulates bacterial activity (Wang et al. 2022). Viral lysis also converts

532 microbial biomass into DOM (Chen et al. 2022). These overlooked sources likely influenced the short-term

533 DOM dynamics in the incubation bottles.

534

535
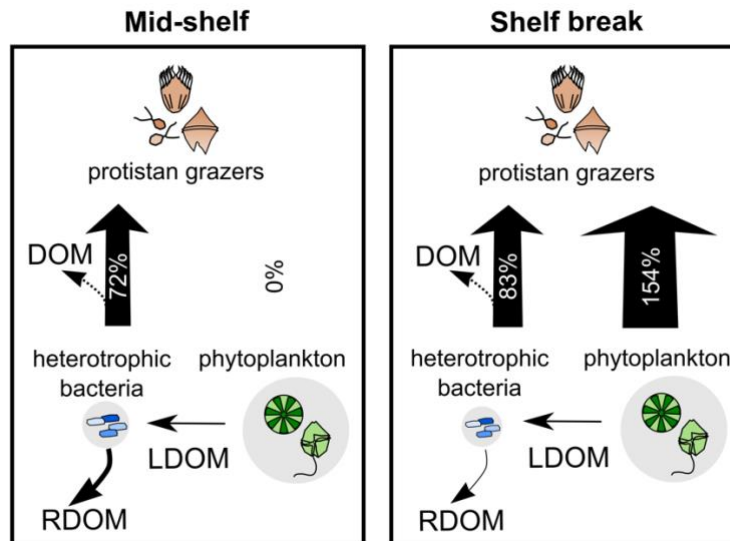
536 **Figure 9. Schematic representation of DOM pathways during the productive season on the Patagonian**

537 **Shelf, contrasting the mid-shelf (low-to-moderate productivity, left panel) with the shelf break front (high**

538 **productivity, right panel). Phytoplankton biomass (background circle size) was twice that of bacteria,**

539 **with selective grazing on bacteria balancing their rapid growth across sampling areas. Grazing on**

540 **phytoplankton increased under higher productivity, aligning with the enhanced microbial loop**

541 **hypothesis. Heterotrophic bacteria were key in shaping DOM quality, utilizing labile DOM (LDOM)**

542 **from phytoplankton and contributing to the storage of refractory DOM (RDOM), even without DOM-**

543 **producing protists. RDOM production was more pronounced mid-shelf than at the shelf break. Bacterial**

544 **grazing influenced the net production of the a254 DOM fraction, with intense grazing leading to DOM**

545 **accumulation likely through reduced bacterial biomass and egested organic material. Arrow thickness**

546 **represents grazing pressure, with percentages indicating daily grazed productivity.**

547

548 The a254 DOM fraction also tended to accumulate under high bacterial mortality due to grazing. Our results

549 evidenced a selective grazing on bacteria compensating for their fast growth rate. This group-specific grazing

550 mortality aligns well with the grazing selectivity model, wherein grazers exhibit preferences against high-

551 growth-rate organisms, establishing a tight coupling between growth advantages and grazing vulnerability

552 across environmental gradients (Landry et al., 2023). Our experimental data not only support this hypothesis

553 but also provide new insights into the repercussions of bacterial grazing on dissolved carbon stocks (Fig. 9).

554 Specifically, our results suggest that grazing on bacteria can lead to an accumulation of DOM produced by

555 phytoplankton by reducing the biomass of bacterial standing stock. In addition, protistan grazing may contribute
556 to the DOM pool by releasing bacterial carbon (Taylor et al., 1985). However, bacteria may not immediately
557 utilize this DOM source, as adapting their enzymatic machinery to target new compounds requires additional
558 energy expenditure, resulting in less efficient resource utilization (Baña et al., 2014). Similar results were
559 observed in polar waters, where high protistan bacterivory was associated with DOM accumulation (Lund
560 Paulsen et al., 2019). Our observations carry biogeochemical implications, as intense bacterial grazing implies
561 that bacterial biomass becomes available to higher trophic levels, thereby circumventing the DOM cycle. In
562 other words, while most bacterial biomass is directed by protistan grazers toward higher trophic levels, it also
563 partially diverts the production of DOM lysates by viral lysis (Suttle, 2005). Our experimental results indicate
564 that the diversion of bacterial carbon from the DOM cycle by protistan grazing is only partial, as protistan
565 grazing introduces additional DOM, while the reduction in bacterial abundance leaves a fraction of
566 phytoplankton-derived DOM unutilized over short timescales.

567 Protistan grazing is widely recognized as the primary driver of phytoplankton mortality (Calbet and Landry,
568 2004) and is an important mortality source for heterotrophic bacteria (Weinbauer and Peduzzi, 1995). However,
569 viral lysis can achieve comparable mortality rates in both phytoplankton and bacterial populations to that caused
570 by protistan grazers. Discerning the viral impact within incubation bottles can be challenging, as viral activity
571 may not only contribute to cell lysis but has been observed to stimulate prey availability for protists, potentially
572 through the release of cellular lysates or by reducing competition (Staniewski and Short, 2014). In our study,
573 while protist grazing was considered the primary cause of bacterial and phytoplankton mortality, we
574 acknowledge that viral lysis may have also played an unrecognized but significant role in the dilution
575 experiments.

576 The fate of grazing-derived DOM remains uncertain in our experimental setup, as it could either serve as a
577 potential source for bacterial utilization, thus establishing positive longer-term predator-prey feedback not
578 captured in our 24-h experiment, or contribute to the complex DOM pool, feeding into the refractory fraction.
579 Indeed, previous observations revealed that DOM derived from protistan grazers varies in its bioavailability
580 (Taylor et al., 1985), and their complexity is further shaped by taxa composition (Nagata and Kirchman, 1992;
581 Gruber et al., 2006). In our experiments, we did not observe a clear trend in DOM transformation between
582 treatments with and without protists, indicating that bacteria remain as the primary drivers of DOM quality.
583 Overall, our finding revealed that under high bacterial growth rate that follows the onset of the productive
584 season, protistan grazers not only channels carbon through remineralization but also, foster the degree of DOM
585 accumulation by reducing DOM-degrading bacterial stock and/or contributing with egestion substances.
586 Additionally, instead of acting solely as a sink of carbon through mineralization of organic compounds, bacteria
587 serve as a crucial link between assimilatory CO_2 and higher trophic levels.

588

589 **Data availability**
590 DOI: 10.5281/zenodo.11662261

591

Authors contribution

CLA conceptualized, designed, and carried out the experiments, analyzed plankton samples and acquired funding. JEGC, AM and ASG analyzed DOC, optical properties of DOM and nutrients samples and interpreted the results. JEGC performed the PARAFAC multivariate algorithm and calculated fluorescence indices. RS analyzed plankton samples and performed biomass calculations. JCM contributed to the numerical methodology design and the conceptualization of overarching goals. LARE analyzed and interpreted CTD data and Moderate Resolution Imaging Spectroradiometer (MODIS) Aqua images of chlorophyll-a. RL coordinated responsibilities for the research activities planning and execution, acquired funding and contributed to the conceptualization of overarching goals. CLA prepared the manuscript with contributions from all co-authors.

Competing interests

The authors declare no competing interests.

Acknowledgments

We are thankful to the crew of the RV "Dr. Bernardo Houssay" of Prefectura Naval Argentina for their support on field activities and sampling. This study was supported by the National Agency for Promotion of Science and Technology (FONCYT-PICT 0467–2010 and FONCYT-PICT 2386-2017), the National Scientific and Technical Research Council (CONICET-PIP 11220200102681CO) and by the Argentine Oceanographic Institute (IADO, CONICET-UNS). The authors acknowledge that language checking and spelling improvements were done by ChatGPT (powered by OpenAI's language model, GPT-3; http://openai.com).

References

Armengol, L., Calbet, A., Franchy, G., Rodríguez-Santos, A., and Hernández-León, S.: Planktonic food web structure and trophic transfer efficiency along a productivity gradient in the tropical and subtropical Atlantic Ocean. Sci Rep, 9, 2044, https://doi.org/10.1038/s41598-019-38507-9, 2019.

Bachi, G., Morelli, E., Gonnelli, M., Balestra, C., Casotti, R., Evangelista, V., Repeta, D. J., and Santinelli, C.: Fluorescent properties of marine phytoplankton exudates and lability to marine heterotrophic prokaryotes degradation, Limnol Oceanogr, 68, https://doi.org/10.1002/lno.12325, 2023.

Bai, Y., Su, R., Han, X., Zhang, C., and Shi, X.: Investigation of seasonal variability of CDOM fluorescence in the southern changjiang river estuary by EEM-PARAFAC, Acta Oceanologica Sinica, 34, 1–12, https://doi.org/10.1007/s13131-015-0714-8, 2015.

Baltar, F., Palovaara, J., Unrein, F., Catala, P., Horňák, K., Šimek, K., Vaqué, D., Massana, R., Gasol, J. M., and Pinhassi, J.: Marine bacterial community structure resilience to changes in protist predation under phytoplankton bloom conditions, ISME J, 10, 568–581, https://doi.org/10.1038/ismej.2015.135, 2016.

Baña, Z., Ayo, B., Marrasé, C., Gasol, J. M., and Iriberri, J.: Changes in bacterial metabolism as a response to dissolved organic matter modification during protozoan grazing in coastal Cantabrian and Mediterranean waters, Environ Microbiol, 16, 498–511, https://doi.org/10.1111/1462-2920.12274, 2014.

630 Banse, K.: Cell volumes, maximal growth rates of unicellular algae and ciliates, and the role of ciliates in the
631   marine pelagial, Limnol Oceanogr, 27, 1059–1071, https://doi.org/10.4319/lo.1982.27.6.1059, 1982.

632 Behrenfeld, M. J. and Boss, E. S.: Student's tutorial on bloom hypotheses in the context of phytoplankton annual
633   cycles. Glob Change Biol, 24, 55–77, https://doi.org/10.1111/gcb.13858, 2018.

634 Berden, G., Charo, M., Möller, O. O., and Piola, A. R.: Circulation and Hydrography in the Western South
635   Atlantic Shelf and Export to the Deep Adjacent Ocean: 30°S to 40°S, J Geophys Res Oceans, 125,
636   https://doi.org/10.1029/2020JC016500, 2020.

637 Berglund, J., Müren, U., Båmstedt, U., and Andersson, A.: Efficiency of a phytoplankton-based and a bacterial-
638   based food web in a pelagic marine system, Limnol Oceanogr, 52, 121–131,
639   https://doi.org/10.4319/lo.2007.52.1.0121, 2007.

640 Brandstetter, A., Sletten, R. S., Mentler, A., and Wenzel, W. W.: Estimating dissolved organic carbon in natural
641   waters by UV absorbance (254 nm), Zeitschrift für Pflanzenernährung und Bodenkunde, 159, 605–
642   607, https://doi.org/10.1002/jpln.1996.3581590612, 1996.

643 Calbet, A.: The trophic roles of microzooplankton in marine systems. ICES J, 65, 325-331,
644   https://doi.org/10.1093/icesjms/fsn013, 2008.

645 Calbet, A. and Landry, M. R.: Phytoplankton growth, microzooplankton grazing, and carbon cycling in marine
646   systems, Limnol Oceanogr Methods, 49, 51–57, https://doi.org/10.4319/lo.2004.49.1.0051, 2004.

647 Calbet, A. and Saiz, E.: How much is enough for nutrients in microzooplankton dilution grazing experiments?,
648   J Plankton Res, 40, 109–117, https://doi.org/10.1093/plankt/fbx070, 2018.

649 Chen, B., Liu, H., Landry, M. R., DaI, M., Huang, B., and Sune, J.: Close coupling between phytoplankton
650   growth and microzooplankton grazing in the western South China Sea, Limnol Oceanogr, 54, 1084–
651   1097, https://doi.org/10.4319/lo.2009.54.4.1084, 2009.

652 Chen, X., Wei, W., Xiao, X., Wallace, D., Hu, C., Zhang, L., Batt, J., Liu, J., Gonsior, M., Zhang, J., LaRoche,
653   J., Hill, P., Xu, D., Wang, J., Jiao, N., and Zhang, R.: Heterogeneous viral contribution to dissolved
654   organic matter processing in a long-term macrocosm experiment. Environ Int, 158, 106950,
655   https://doi.org/10.1016/j.envint.2021.106950, 2022.

656 Chiang, K.-P., Tsai, A.-Y., Tsai, P.-J., Gong, G.-C., Huang, B.-Q., and Tsai, S.-F.: The influence of
657   nanoflagellates on the spatial variety of picoplankton and the carbon flow of the microbial food web
658   in the oligotrophic subtropical pelagic continental shelf ecosystem, Cont Shelf Res, 80, 57–66,
659   https://doi.org/10.1016/j.csr.2014.02.019, 2014.

660 Coble, P. G.: Characterization of marine and terrestrial DOM in seawater using excitation-emission matrix
661   spectroscopy, Mar Chem, 51, 325–346, https://doi.org/10.1016/0304-4203(95)00062-3, 1996.

662 Delgado, A. L., Hernández-Carrasco, I., Combes, V., Font-Muñoz, J., Pratolongo, P. D., and Basterretxea, G.:
663   Patterns and Trends in Chlorophyll-a Concentration and Phytoplankton Phenology in the
664   Biogeographical Regions of Southwestern Atlantic, J Geophys Res Oceans, 128,
665   https://doi.org/10.1029/2023JC019865, 2023.

Drozdova, A. N., Krylov, I. N., Nedospasov, A. A., Arashkevich, E. G., and Labutin, T. A.: Fluorescent signatures of autochthonous dissolved organic matter production in Siberian shelf seas. Front Mar Sci 9:872557. https://doi:10.3389/fmars.2022.872557, 2022.

Ferronato, C., Berden, G., Rivarossa, M., and Guinder, V. A.: Wind-driven currents and water masses shape spring phytoplankton distribution and composition in hydrologically complex, productive shelf waters, Limnol Oceanogr, 68, 2195–2210, https://doi.org/10.1002/lno.12413, 2023.

Garzón-Cardona, J. E., Guinder, V. A., Alonso, C., Martínez, A. M., Pantoja-Gutiérrez, S., Kopprio, G. A., Krock, B., and Lara, R. J.: Chemically unidentified dissolved organic carbon: A pivotal piece for microbial activity in a productive area of the Northern Patagonian shelf, Mar Environ Res, 167, 105286, https://doi.org/10.1016/j.marenvres.2021.105286, 2021.

Goericke, R.: The structure of marine phytoplankton communities-patterns, rules and mechanisms, California Cooperative Oceanic Fisheries Investigation Reports, 52, 182–197, 2011.

Görs, S., Rentsch, D., Schiewer, U., Karsten, U., and Schumann, R.: Dissolved organic matter along the eutrophication gradient of the Darβ–Zingst Bodden Chain, Southern Baltic Sea: I. Chemical characterisation and composition. Mar Chem, 104, 125-142, https://doi.org/10.1016/j.marchem.2006.10.009, 2007.

Gruber, D. F., Simjouw, J.-P., Seitzinger, S. P., and Taghon, G. L.: Dynamics and characterization of refractory dissolved organic matter produced by a pure bacterial culture in an experimental predator-prey system, Appl Environ Microbiol, 72, 4184–4191, https://doi.org/10.1128/AEM.02882-05, 2006.

Hach, P. F., Marchant, H. K., Krupke, A., Riedel, T., Meier, D. V., Lavik, G., Holtappels, M., Dittmar, T., and Kuypers, M. M. M.: Rapid microbial diversification of dissolved organic matter in oceanic surface waters leads to carbon sequestration, Sci Rep, 10, 13025, https://doi.org/10.1038/s41598-020-69930-y, 2020.

Häder, D. P., Williamson, C. E., Wängberg, S. Å., Rautio, M., Rose, K. C., Gao, K., Helbling, W. E., Sinha, R. P., and Worrest, R.: Effects of UV radiation on aquatic ecosystems and interactions with other environmental factors. Photochem Photobiol Sci, 14(1), 108-126, https://doi:10.1039/c4pp90035a, 2015.

Hansell, D. A., Carlson, C. A., Repeta, D. J., and Schlitzer, R.: Dissolved organic matter in the ocean: A controversy stimulates new insights. Oceanography, 22, 202-211, https://doi.org/10.5670/oceanog.2009.109, 2009.

Hansen, P. J., Bjørnsen, P. K., and Hansen, B. W.: Zooplankton grazing and growth: Scaling within the 2-2,000-μm body size range. Limnol Oceanogr, 42, 687-704, https://doi.org/10.4319/lo.1997.42.4.0687, 1997.

Hillebrand, H., Dürselen, C., Kirschtel, D., Pollingher, U., and Zohary, T.: Biovolume calculation for pelagic and benthic microalgae, J Phycol, 35, 403–424, https://doi.org/10.1046/j.1529-8817.1999.3520403.x, 1999.

Hozbor, M. C., Hernández, D. R., Cucchi Colleoni, A. D., Costagliola, M. C., and Peressutti, S. R.: Biomasa y distribución espacial del bacterioplancton en el sector norte de la plataforma continental argentina (34º S-41º S), Revista de Investigación y Desarrollo Pesquero, 23, 145–160, 2013.

704 Huguet, A., Vacher, L., Relexans, S., Saubusse, S., Froidefond, J. M., and Parlanti, E.: Properties of fluorescent
705   dissolved organic matter in the Gironde Estuary, Org Geochem, 40, 706–719,
706   https://doi.org/10.1016/j.orggeochem.2009.03.002, 2009.

707 Hutchins, D. A. and Fu, F.: Microorganisms and ocean global change, Nat Microbiol, 2, 17058,
708   https://doi.org/10.1038/nmicrobiol.2017.58, 2017.

709 Irigoien, X., Flynn, K. J., and Harris, R. P.: Phytoplankton blooms: a 'loophole' in microzooplankton grazing
710   impact?, J Plankton Res, 27, 313–321, https://doi.org/10.1093/plankt/fbi011, 2005.

711 Jeffrey, S. W. and Humphrey, G. F.: New spectrophotometric equations for determining chlorophylls a, b, c1
712   and c2 in higher plants, algae and natural phytoplankton, Biochemie und Physiologie der Pflanzen,
713   167, 191–194, https://doi.org/10.1016/S0015-3796(17)30778-3, 1975.

714 Jiao, N., Herndl, G. J., Hansell, D. A., Benner, R., Kattner, G., Wilhelm, S. W., Kirchman, D. L., Weinbauer,
715   M. G., Luo, T., Chen, F., and Azam, F.: Microbial production of recalcitrant dissolved organic matter:
716   long-term carbon storage in the global ocean. Nat Rev Microbiol, 8, 593–599,
717   https://doi.org/10.1038/nrmicro2386, 2010.

718 Jørgensen, L., Stedmon, C. A., Kragh, T., Markager, S., Middelboe, M., and Søndergaard, M.: Global trends in
719   the fluorescence characteristics and distribution of marine dissolved organic matter. Mar Chem, 126(1–
720   4), 139–148, https://doi.org/10.1016/j.marchem.2011.05.002, 2011.

721 Kahl, L. C., Bianchi, A. A., Osiroff, A. P., Pino, D. R., and Piola, A. R.: Distribution of sea-air CO2 fluxes in
722   the Patagonian Sea: Seasonal, biological and thermal effects, Cont Shelf Res, 143, 18–28,
723   https://doi.org/10.1016/j.csr.2017.05.011, 2017.

724 Kanayama, T., Kobari, T., Suzuki, K., Yoshie, N., Honma, T., Karu, F., and Kume, G.: Impact of
725   microzooplankton grazing on the phytoplankton community in the Kuroshio of the East China sea: A
726   major trophic pathway of the Kuroshio ecosystem, Deep-Sea Res I: Oceanogr Res Pap, 163, 103337,
727   https://doi.org/10.1016/j.dsr.2020.103337, 2020.

728 Kang, H. C., Jeong, H. J., Ok, J. H., Lim, A. S., Lee, K., You, J. H., Park, S. A., Eom, S. H., Lee, S. Y., Lee, K.
729   H., Jang, S. H., Yoo, Y. Du, Lee, M. J., and Kim, K. Y.: Food web structure for high carbon retention
730   in marine plankton communities, Sci Adv, 9, https://doi.org/10.1126/sciadv.adk0842, 2023.

731 Kattner, G. and Becker, H.: Nutrients and organic nitrogenous compounds in the marginal ice zone of the Fram
732   Strait, J Mar Syst, 2, 385–394, https://doi.org/10.1016/0924-7963(91)90043-T, 1991.

733 Kinsey, J. D., Corradino, G., Ziervogel, K., Schnetzer, A., and Osburn, C. L.: Formation of chromophoric
734   dissolved organic matter by bacterial degradation of phytoplankton-derived aggregates, Front Mar Sci,
735   4, https://doi.org/10.3389/fmars.2017.00430, 2018.Kujawinski, E. B., Del Vecchio, R., Blough, N. V.,
736   Klein, G. C., and Marshall, A. G.: Probing molecular-level transformations of dissolved organic
737   matter: insights on photochemical degradation and protozoan modification of DOM from electrospray
738   ionization Fourier transform ion cyclotron resonance mass spectrometry, Mar Chem, 92, 23–37,
739   https://doi.org/10.1016/j.marchem.2004.06.038, 2004.

740 Landry, M. R. and Hassett, R. P.: Estimating the grazing impact of marine micro-zooplankton, Mar Biol, 67,
741   283–288, https://doi.org/10.1007/BF00397668, 1982.

Landry, M. R., Stukel, M. R., Selph, K. E., and Goericke, R.: Coexisting picoplankton experience different relative grazing pressures across an ocean productivity gradient, Proc Natl Acad Sci USA, 120, https://doi.org/10.1073/pnas.2220771120, 2023.

Laruelle, G. G., Cai, W.-J., Hu, X., Gruber, N., Mackenzie, F. T., and Regnier, P.: Continental shelves as a variable but increasing global sink for atmospheric carbon dioxide, Nat Commun, 9, 454, https://doi.org/10.1038/s41467-017-02738-z, 2018.

Laws, E. A, Landry, M. R., Barber, R. T., Campbell, L., Dickson, M.-L., and Marra J.: Carbon cycling in primary production bottle incubations: Inferences from grazing experiments and photosynthetic studies using ^{14}C and ^{18}O in the Arabian Sea, Deep Sea Res Part II, 47, 1339-1352, https://doi.org/10.1016/S0967-0645(99)00146-0, 2000.

Lechtenfeld, O. J., Hertkorn, N., Shen, Y., Witt, M., and Benner, R.: Marine sequestration of carbon in bacterial metabolites, Nat Commun, 6, 6711, https://doi.org/10.1038/ncomms7711, 2015.

Lee, M.-H., Osburn, C. L., Shin, K.-H., and Hur, J.: New insight into the applicability of spectroscopic indices for dissolved organic matter (DOM) source discrimination in aquatic systems affected by biogeochemical processes, Water Res, 147, 164–176, https://doi.org/10.1016/j.watres.2018.09.048, 2018.

Lehahn, Y., d'Ovidio, F., and Koren, I.: A Satellite-Based Lagrangian View on Phytoplankton Dynamics, Ann Rev Mar Sci, 10, 99–119, https://doi.org/10.1146/annurev-marine-121916-063204, 2018.

Lønborg, C., Álvarez-Salgado, X. A., Davidson, K., Martínez-García, S., and Teira, E.: Assessing the microbial bioavailability and degradation rate constants of dissolved organic matter by fluorescence spectroscopy in the coastal upwelling system of the Ría de Vigo, Mar Chem, 119, 121–129, https://doi.org/10.1016/j.marchem.2010.02.001, 2010.

Lønborg, C., Yokokawa, T., Herndl, G. J., and Antón Álvarez-Salgado, X.: Production and degradation of fluorescent dissolved organic matter in surface waters of the eastern north Atlantic ocean, Deep Sea Res Part I: Oceanog Res Pap, 96, 28–37, https://doi.org/10.1016/j.dsr.2014.11.001, 2015.

Lucas, A. J., Guerrero, R. A., Mianzán, H. W., Acha, E. M., and Lasta, C. A.: Coastal oceanographic regimes of the Northern Argentine Continental Shelf (34–43°S), Estuar Coast Shelf Sci, 65, 405–420, https://doi.org/10.1016/j.ecss.2005.06.015, 2005.

Lund Paulsen, M., Müller, O., Larsen, A., Møller, E. F., Middelboe, M., Sejr, M. K., and Stedmon, C.: Biological transformation of Arctic dissolved organic matter in a NE Greenland fjord, Limnol Oceanogr, 64, 1014–1033, https://doi.org/10.1002/lno.11091, 2019.

Martínez-Pérez, A. M., Nieto-Cid, M., Osterholz, H. Catalá, T.S., Reche, I., Dittmar, T., and Álvarez-Salgado, J. A.: Linking optical and molecular signatures of dissolved organic matter in the Mediterranean Sea. Sci Rep 7, 3436, https://doi.org/10.1038/s41598-017-03735-4, 2017.

McCauley, D. J., Gellner, G., Martinez, N. D., Williams, R. J., Sandin, S. A., Micheli, F., Mumby, P. J., and McCann, K. S.: On the prevalence and dynamics of inverted trophic pyramids and otherwise top-heavy communities, Ecol Lett, 21, 439–454, https://doi.org/10.1111/ele.12900, 2018.

779 McKnight, D. M., Boyer, E. W., Westerhoff, P. K., Doran, P. T., Kulbe, T., and Andersen, D. T.:
780   Spectrofluorometric characterization of dissolved organic matter for indication of precursor organic
781   material and aromaticity, Limnol Oceanogr, 46, 38–48, https://doi.org/10.4319/lo.2001.46.1.0038,
782   2001.

783 Moran, M. A., Ferrer-González, F. X., Fu, H., Nowinski, B., Olofsson, M., Powers, M. A., Schreier, J. E.,
784   Schroer, W. F., Smith, C. B. and Uchimiya, M.: The Ocean's labile DOC supply chain. Limnol
785   Oceanogr, 67, 1007-1021, https://doi.org/10.1002/lno.12053, 2022.

786 Nagata, T. and Kirchman, D.: Release of macromolecular organic complexes by heterotrophic marine
787   flagellates, Mar Ecol Prog Ser, 83, 233–240, https://doi.org/10.3354/meps083233, 1992.

788 Negri, R. M., Silva, R. I., Segura, V., and Cucchi Colleoni, A. D.: Estructura de la comunidad del fitoplancton
789   en el área de El Rincón, Mar Argentino (febrero 2011), Revista Investigación Desarrollo Pesquero, 23,
790   7–22, 2013.

791 Negri, R. M., Molinari, G., Carignan, M., Ortega, L., Ruiz, M. G., Cozzolino, E., Cucchi-Colleoni, A. D., Lutz,
792   V. A., Costagliola, M., Garcia, A. B., Izzo, S., Jurquiza, V., Salomone, A., Odizzio, M., La Torre, S.,
793   Sanabria, A., Hozbor, M. C., Peressutti, S. R., Méndez, S. M., Silva, R., Martínez, A., Cepeda, G. D.,
794   Viñas, M. D., Diaz, M. V., Pajaro, M., Mattera, M. B., Montoya, N. G., Berghoff, C., and Leonarduzzi,
795   E.: Ambiente y plancton en la zona Común de pesca argentino-uruguaya en un escenario de cambio
796   climático (marzo, 2014), Publicaciones de la Comisión Técnica Mixta del Frente Marítimo, 251–316,
797   2016.

798 Orselli, I. B. M., Kerr, R., Ito, R. G., Tavano, V. M., Mendes, C. R. B., and Garcia, C. A. E.: How fast is the
799   Patagonian shelf-break acidifying?, J Mar Syst, 178, 1–14,
800   https://doi.org/10.1016/j.jmarsys.2017.10.007, 2018.

801 Osburn, C. L., Kinsey, J. D., Bianchi, T. S., and Shields, M. R.: Formation of planktonic chromophoric
802   dissolved organic matter in the ocean, Mar Chem, 209, 1–13,
803   https://doi.org/10.1016/j.marchem.2018.11.010, 2019.

804 Paparazzo, F. E., Bianucci, L., Schloss, I. R., Almandoz, G. O., Solís, M., and Esteves, J. L.: Cross-frontal
805   distribution of inorganic nutrients and chlorophyll-a on the Patagonian Continental Shelf of Argentina
806   during summer and fall. Revista de Biología Marina y Oceanografía, 45, 107–119.
807   http://dx.doi.org/10.4067/S0718-19572010000100010, 2010.

808 Porter, K. G. and Feig, Y. S.: The use of DAPI for identifying and counting aquatic microflora1, Limnol
809   Oceanogr, 25, 943–948, https://doi.org/10.4319/lo.1980.25.5.0943, 1980.

810 Redfield, A. C., Ketchum, B. H., and Richards, F. A.: The influence of organisms on the composition of sea-
811   water, in: The sea: ideas and observations on progress in the study of the seas, vol. 2, edited by: Hill,
812   M. N., Wiley Interscience, New York, 26–77, 1963.

813 Romera-Castillo, C., Sarmento, H., Álvarez-Salgado, X. A., Gasol, J. M., and Marraséa, C.: Production of
814   chromophoric dissolved organic matter by marine phytoplankton, Limnol Oceanogr, 55, 446–454,
815   https://doi.org/10.4319/lo.2010.55.1.0446, 2010.

816 Romera-Castillo, C., Sarmento, H., Álvarez-Salgado, X. A., Gasol, J. M., and Marrasé, C.: Net production and
817   consumption of fluorescent colored dissolved organic matter by natural bacterial assemblages growing
818   on marine phytoplankton exudates, Appl Environ Microbiol, 77, 7490–7498,
819   https://doi.org/10.1128/AEM.00200-11, 2011.

820 Romero, S. I., Piola, A. R., Charo, M., and Garcia, C. a. E.: Chlorophyll- a variability off Patagonia based on
821   SeaWiFS data, J Geophys Res, 111, 1–11, https://doi.org/10.1029/2005JC003244, 2006.

822 Sanders, R., Caron, D., and Berninger U, G.: Relationships between bacteria and heterotrophic nanoplankton
823   in marine and fresh waters: an inter-ecosystem comparison, Mar Ecol Prog Ser, 86, 1–14,
824   https://doi.org/10.3354/meps086001, 1992.

825 Saraceno, M., Bodnariuk, N., Ruiz-Etcheverry, L. A., Berta, M., Simionato, C. G., Beron-Vera, F. J., and
826   Olascoaga, M. J.: Lagrangian characterization of the southwestern Atlantic from a dense surface drifter
827   deployment, Deep Sea Res Part I: Oceanog Res Pap, 208, 104319,
828   https://doi.org/10.1016/j.dsr.2024.104319, 2024.

829 Sarmento, H., Morana, C., and Gasol, J. M.: Bacterioplankton niche partitioning in the use of phytoplankton-
830   derived dissolved organic carbon: quantity is more important than quality, ISME J, 10, 2582–2592,
831   https://doi.org/10.1038/ismej.2016.66, 2016.

832 Sherr, E. B. and Sherr, B. F.: Heterotrophic dinoflagellates: a significant component of microzooplankton
833   biomass and major grazers of diatoms in the sea. Mar Ecol Prog Ser, 352, 187-197,
834   https://doi:10.3354/meps07161, 2007.

835 Sieburth, J. McN., Smetacek, V., and Lenz, J.: Pelagic ecosystem structure: Heterotrophic compartments of the
836   plankton and their relationship to plankton size fractions, Limnol Oceanogr, 23, 1256–1263,
837   https://doi.org/10.4319/lo.1978.23.6.1256, 1978.

838 Silva, R., Negri, R., and Lutz, V.: Summer succession of ultraphytoplankton at the EPEA coastal station
839   (Northern Argentina), J Plankton Res, 31, 447–458, https://doi.org/10.1093/plankt/fbn128, 2009.

840 Simon, M. and Azam, F.: Protein content and protein synthesis rates of planktonic marine bacteria, Mar Ecol
841   Prog Ser, 51, 201–213, https://doi.org/10.3354/meps051201, 1989.

842 Skoog, A., Thomas, D., Lara, R., and Richter, K.-U.: Methodological investigations on DOC determinations by
843   the HTCO method, Mar Chem, 56, 39–44, https://doi.org/10.1016/S0304-4203(96)00084-9, 1997.

844 Song, H., Marshall, J., Follows, M. J., Dutkiewicz, S., and Forget, G.: Source waters for the highly productive
845   Patagonian shelf in the southwestern Atlantic. J Mar Syst, 158, 120–128,
846   https://doi.org/10.1016/j.jmarsys.2016.02.009, 2016.

847 Spencer, R. G. M., Pellerin, B. A., Bergamaschi, B. A., Downing, B. D., Kraus, T. E. C., Smart, D. R., Dahlgren,
848   R. A., and Hernes, P. J.: Diurnal variability in riverine dissolved organic matter composition
849   determined by *in situ* optical measurement in the San Joaquin River (California, USA), Hydrol Process,
850   21, 3181–3189, https://doi.org/10.1002/hyp.6887, 2007.

851 Staniewski, M. A. and Short, S. M.: Potential viral stimulation of primary production observed during
852   experimental determinations of phytoplankton mortality. Aquat Microb Ecol, 71, 239-256,
853   https://doi.org/10.3354/ame01679, 2014.

Stedmon, C. A. and Bro, R.: Characterizing dissolved organic matter fluorescence with parallel factor analysis: a tutorial, Limnol Oceanogr Methods, 6, 572–579, https://doi.org/10.4319/lom.2008.6.572, 2008.

Stedmon, C. A., Markager, S., and Bro, R.: Tracing dissolved organic matter in aquatic environments using a new approach to fluorescence spectroscopy. Mar Chem, 82(3-4), 239-254, https://doi.org/10.1016/S0304-4203(03)00072-0, 2003.

Suttle, C. A.: Viruses in the sea, Nature, 437, 356–361, https://doi.org/10.1038/nature04160, 2005.

Taylor, A. and Landry, M.: Phytoplankton biomass and size structure across trophic gradients in the southern California Current and adjacent ocean ecosystems, Mar Ecol Prog Ser, 592, 1–17, https://doi.org/10.3354/meps12526, 2018.

Taylor, G. T., Iturriaga, R., and Sullivan, C. W.: Interactions of bactivorous grazers and heterotrophic bacteria with dissolved organic matter, Mar Ecol Prog Ser, 60, 1884–1888, https://doi.org/10.3354/meps023129, 1985.

Tremaine, S. C. and Mills, A. L.: Tests of the critical assumptions of the dilution method for estimating bacterivory by microeucaryotes, Appl Environ Microbiol, 53, 2914–2921, https://doi.org/10.1128/aem.53.12.2914-2921.1987, 1987.

Urban-Rich, J., McCarty, J. T., and Shailer, M.: Effects of food concentration and diet on chromophoric dissolved organic matter accumulation and fluorescent composition during grazing experiments with the copepod Calanus finmarchicus, ICES J Mar Sci, 61, 542–551, https://doi.org/10.1016/j.icesjms.2004.03.024, 2004.

Wang, Y., Xie, R., Shen, Y., Cai, R., He, C., Chen, Q., Guo, W., Shi, Q., Jiao, N., Zheng, Q.: Linking microbial population succession and DOM molecular changes in *Synechococcus*-derived organic matter addition incubation. Microbiol Spectr, 10(2): e0230821, https://doi:10.1128/spectrum.02308-21, 2022.

Weinbauer, M. G. and Peduzzi, P.: Significance of viruses versus heterotrophic nanoflagellates for controlling bacterial abundance in the northern Adriatic Sea, J Plankton Res, 17, 1851–1856, https://doi.org/10.1093/plankt/17.9.1851, 1995.